



A Journal of



Accepted Article

Title: Rational synthesis of tetrahydrodibenzophenanthridine and phenanthroimidazole as efficient blue emitters and its applications

Authors: Manojkumar Dhanthala Thiyagarajan, Umamahesh Balijapalli, Sohrab Nasiri, Dmytro Volyniuk, Jurate Simokaitienec, Madhvesh Pathak, Sathiyarayanan Kulathu Iyer, and Juozas Vidas Gražulevičius

This manuscript has been accepted after peer review and appears as an Accepted Article online prior to editing, proofing, and formal publication of the final Version of Record (VoR). This work is currently citable by using the Digital Object Identifier (DOI) given below. The VoR will be published online in Early View as soon as possible and may be different to this Accepted Article as a result of editing. Readers should obtain the VoR from the journal website shown below when it is published to ensure accuracy of information. The authors are responsible for the content of this Accepted Article.

To be cited as: *Eur. J. Org. Chem.* 10.1002/ejoc.201901711

Link to VoR: <http://dx.doi.org/10.1002/ejoc.201901711>

Supported by



WILEY-VCH

Rational synthesis of tetrahydrodibenzophenanthridine and phenanthroimidazole as efficient blue emitters and its applications

Mr. Manojkumar Dhanthala Thiyagarajan ^a, Dr. Umamahesh Balijapalli ^{a, b}, Mr. Sohrab Nasiri ^c, Dr. Dmytro Volyniuk ^c, Dr. Jurate Simokaitienec ^c, Prof. Madhvesh Pathak ^{*a}, Prof. Sathiyarayanan Kulathu Iyer ^{*a} and Prof. Juozas Vidas Gražulevičius ^{*c}

Abstract: Ten luminophores based on tetrahydrodibenzophenanthridine (THDP) and phenanthroimidazole (PI) were designed, synthesized and characterized for their thermal, electrochemical, electro-optical, charge-transporting characteristics and electroluminescent properties. The blue luminophores exhibited high photoluminescence quantum yields of 66-93% in toluene solutions and of 5-59% in solid films. The highest values were observed for the derivative of THDP and PI containing methoxy group. The compounds showed close values of ionization potentials (5.74-6.11 eV) and electron affinities (2.71-3.06 eV). The selected compounds were tested in electroluminescent devices for the preparation of non-doped light-emitting layers. The best device fabricated using derivative of THDP and PI with methoxy groups showed blue electroluminescence with brightness of 10000 cd/m² at high applied voltages. We performed DFT calculations, and observed lowest singlet-triplet gap (ΔE_{ST}) values of 0.33 and 0.03 eV, oscillator strength (*f*) values of 0.034 and 0.008 for CN and NO₂ derivatives. Interestingly, we observed that compounds **3g** and **3i** showed HOMO and LUMO levels of almost similar energy gap (*E_g*) of 3.60 eV and we observed deeper HOMO values of -5.30, -5.33 eV and LUMO values of -1.94, -2.77 eV.

Introduction

Organic light-emitting diodes (OLEDs) have drawn massive attention due to their increasing applications in flat-panel displays and lighting devices.^[1] OLEDs can be driven at low voltages to produce high brightness, wide viewing angles, fast response, low power consumption light-weight,^[2] industrial and professional displays and micro-display products have already been developed. Researchers have reported deep-blue phosphorescent materials.^[3,4] Phosphorescent OLEDs can theoretically achieve 100% internal quantum efficiency. However, blue phosphorescent OLEDs have short lifetime and sharp efficiency roll-off at high brightness.^[5] The fabrication of OLEDs

can be done by two distinct methods, namely wet and dry processes. Typically, dry-process is used to realize high efficiency OLEDs with high-quality light.^[6-8] Shortcomings such as inefficient use of materials, high energy consumption and poor scalability are major issues in cost-effective, mass-production.

In contrast, some of the aforementioned approaches can be adopted in wet-process to fabricate high-quality light OLED devices, but with comparatively low efficiency. Nevertheless, wet-process is deemed far superior in enabling simple fabrication, large area-size and roll-to-roll production, and consequently more cost-effective. However, energetic doping often requires minute control of doping concentration and inescapably increases manufacturing cost and this type of phase separation in the dopant-host system can make energy transfer ineffective. Many recent researchers have reported a high efficiency of blue fluorescent materials.^[9-12] Some of them offer deep-blue emission with CIE_y<0.10.^[13] Recently, Benzimidazole-based materials that possess different functional chromophores have been demonstrated as deep-blue-light emitters.^[14] However, these materials have deep HOMO, thereby leading to larger hole-injection barriers at the hole-transporter emitter junctions, and thus they require higher operation voltages and provide lower efficiencies.^[15-16] In fact, deep-blue OLEDs with high efficiency, good color stability, and low working voltage are rare.^[17-20]

Tetrahydrodibenzophenanthridine (THDP) is a well-known fluorophore with exceptional photophysical properties, used as intermediate for the construction of organometallics and also utilized as a ratiometric fluorescence sensor for the detection of aniline.^[21] On the other hand, 1,3,5-tris(*N*-phenylbenzimidazol-2-yl)benzene (TPBi) was widely used as an electron-injection and hole-blocking material in OLEDs. However, due to localization of its emission in the ultraviolet spectral region (368 nm), TPBi can not be used as an emitter. Phenanthro[9,10-*d*]imidazole (PI) containing imidazole unit exhibits excellent thermal stability, highly efficient photoluminescence (PL) quantum yields and balanced charge carrier injection properties which make derivatives of PI promising candidates for OLEDs.^[22] This information inspired us to develop new derivatives of THDP and PI as blue materials by a facile synthetic processes followed by systematic studies of their thermal, photophysical, and charge injection properties. In addition, postfunctionalization of derivatives of THDP and PI was performed by functional groups such as NO₂, CN, methoxy, methyl, and by halogens.

In this work, we used the donor- π -acceptor approach to design new molecules with PI core as the acceptor for its good electron-transporting mobility and THDP as the donor for good hole transport mobility and for connecting them with different linkers.^[23-26] New THDP and PI derivative containing methoxy group

- [a] Mr. Manojkumar Dhanthala Thiyagarajana, Prof. Madhvesh Pathak, Prof. Sathiyarayanan Kulathu Iyer, Department of Chemistry, School of Advanced Sciences, Vellore Institute of Technology, Vellore-632014, Tamilnadu, India. E-mail: sathiya_kuna@hotmail.com and madhveshpathak@vit.ac.in
<https://www.sites.google.com/site/sathiyarayananresearchgroup/home?authuser=0>
- [b] Dr. Umamahesh Balijapallia, Centre for Organic Photonics and Electronics Research (OPERA), Kyushu University, 744 Motooka, Nishi, Fukuoka 819-0395, Japan.
<http://www.cstf.kyushu-u.ac.jp/~adachilab/lab/>
- [c] Mr. Sohrab Nasiric, Dr. Dmytro Volyniukc, Dr. Jurate Simokaitienec, Prof. Juozas Vidas Gražulevičius Kaunas University of Technology, Department of Polymer Chemistry and Technology, Radvilenu pl.19, LT 50254, Kaunas, Lithuania, E-mail: juozas.grazulevicius@ktu.lt
<https://fct.ktu.edu/departament-of-polymer-chemistry-and-technology/>

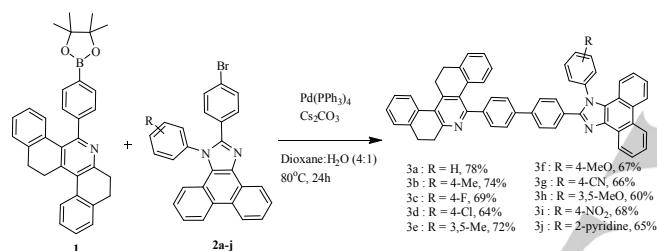
Supporting information for this article is given via a link at the end of the document.

FULL PAPER

showed the highest photoluminescence quantum yields in both toluene solutions (93 %) and in solid state (59 %). The best device performance was observed using non-doped light-emitting layer of this compound.

Synthesis and Characterization

THDP was easily prepared by the one-pot condensation reaction of substituted aldehydes, ammonium acetate and 2-tetralone with good yields.^[27] 5-(4-(4,4,5,5-tetramethyl-1,3,2-dioxaborolan-2-yl)phenyl)-7,8,13,14-tetrahydrodi benzo[a,i] phenanthridine (**BTHDP**) which is a key intermediate (its chemical structure shown in **Scheme 1**) was synthesized in good yield of 65% according to the previously reported procedure (see the experimental section for the details).^[28] The reaction of 9, 10-phenanthrenequinone, p-bromobenzaldehyde with substituted aniline derivatives in the presence of ammonium acetate, and acetic acid gave substituted bromophenyl phenanthroimidazoles (**BrPI**) as yellow solids with up to 90% yields (see supporting information).



Scheme 1: Synthesis of 5-(4'-(1-phenyl-1H-phenanthro[9,10-d]imidazol-2-yl)-[1,1'-biphenyl]-4-yl)-7,8,13,14-tetrahydrodibenzo[a,i]phenanthridine and its derivatives.

In the final step, we used palladium-catalyzed Suzuki coupling to couple **BTHDP** with **BrPI** derivatives to obtain **THDP-PI** bipolar fluorophores (**3a-3j**) as shown in Scheme 1. The optimized reaction conditions were established by the screening of catalyst, solvent, base, temperature. The details were given in Table S1 in supporting information. It found out that 10 mol% Pd(PPh₃)₄ and 2 eq of Cs₂CO₃ in dioxane/H₂O (4:1) allowed to obtain compound **3a** in 78% yield (Table S1). Functional groups such as NO₂, CN, methoxy, methyl, and halogens tolerated the reaction conditions and the coupling smoothly proceeded to produce the desired compounds in good yields. All the compounds were freely soluble in common organic solvents and were purified by column chromatography using a mixture of ethylacetate/chloroform /n-hexane as the eluent. Further, the purity was improved by consecutive crystallization steps and the structures were ascertained by FTIR, NMR, and mass spectrometry analysis (see section 1, supporting information).

Photophysical properties

To investigate the effect of the substitution pattern on photophysical properties of the THDPs and PI derivatives, absorption and photoluminescent (PL) spectra of their solutions and solid films were recorded (Figure 1a-d and Figure S1). Low-energy bands of absorption spectra of toluene solutions of all derivatives were characterized by maxima at 346-361 nm and low-intensity shoulder at 365-375nm. These absorption bands can be mainly attributed to absorption of PI moiety, since the lowest energy band is situated at the same region (with maximum at 364 nm) and is red-shifted in comparison to the lowest energy band (with maximum at 318 nm) of BTHDPs (Table 1).^[29-33] Small blue-shifts of the maxima of the lowest energy bands of compounds **3a-j** relative to that of PI is, apparently, the result of superposition of absorption spectra of both donating and accepting units. Additional red-shifted energy bands (shoulders) that indicate intramolecular charge transfer (ICT) transitions in ground states between donor and acceptor units were practically not observed because of the presence of diphenyl spacers between THDP and PI moieties. As a result, similar optical energy band gaps (E_g^{opt}) were obtained for the studied compounds (Table 1). Slight differences in the position of the lowest absorption bands were observed for the toluene solutions of derivatives **3a-j** due to their post-functionalization's by different moieties inducing different steric and polar effects, which affected electron delocalization. A similar absorption behavior of the derivatives **3a-j** was also observed more in polar solvents than in toluene, revealing their weak solvatochromic effects in ground states. Absorption spectra of solid films of **3a-j** practically reconstituted the corresponding spectra which were only slightly red-shifted due to the aggregation effects of the solutions (Figure 1b). Intensive, deep-blue fluorescence with high photoluminescence quantum yield (PLQY) was observed for toluene solutions of compounds **3a-j** (Table 1). The highest PLQY value of 93 % was recorded for toluene solution of compound **3f** containing methoxy substituent. PL decays of the toluene solutions were agreed well with the mono-exponential law (Figure 1c and 2). Close to nanosecond, life times of fluorescence were observed for all the solutions, displaying weak effect of the substitution pattern (Table 1). For adequate description of PL decay curves of the films of compounds, double or triple exponentials fits were required. The reasons of different PL decays of the films from those solutions could be due to aggregation induced quenching and/or excimer formation. Clear effect of substitution pattern on PL decays of the films of **3a-j** was observed (Figure 1c, 2 and Table 1). Different shapes of PL decays of the films **3a-j** may partly be related to non-radiative losses in solid-state. Indeed, much lower PLQY values of solid samples of **3a-j** were obtained in a comparison to those of their toluene solutions (Table 1). Compound **3f**, containing methoxy group, demonstrated relatively high PLQY of 59% in solid-state. It was higher than that of compound **3a**, which did not have any substituent at phenyl group linked to PI moiety. High PLQY of solid sample of **3f** can be related to restriction of excimer formation, which may occur between planar moieties, as it was shown elsewhere.^[34]

FULL PAPER

Table 1. Photophysical parameters of the solutions of compounds **3a-j** in toluene and solid films.

Compounds	λ_{abs}^{max} , nm	E_g^{opt} , eV	λ_F^{max} , nm	τ , ns	PLQY, %	FWHM, nm	CIE1931, (x, y)	Slope ^a , cm ⁻¹
	Toluene/film							
3a	348/352	3.03/2.76	417, 435/ 463	0.92/ 0.13, 7.33	93/27	77/125	(0.154, 0.059)/ (0.202, 0.249)	7513
3b	346/351	3.01/2.79	417, 434/ 480	0.96/ 0.68, 4.43	67/11	67/126	(0.156, 0.063)/ (0.204, 0.176)	6931
3c	347/355	3.05/2.79	415, 434/ 465	0.95/ 0.21, 2.04, 8.12	87/32	69/128	(0.156, 0.056)/ (0.202, 0.249)	2958
3d	345/355	3.02/2.78	416, 434/ 502	1.02/ 0.09, 1.72, 7.49	66/8	67/131	(0.157, 0.063)/ (0.236, 0.349)	2633
3e	348/352	3.01/2.78	418, 435/ 503	1.02/ 0.11, 1.90, 7.89	75/12	68/135	(0.157, 0.065)/ (0.230, 0.335)	3846
3f	349/351	3.02/2.77	418, 434/ 480	0.93/ 0.13, 1.56, 8.27	93/59	66/137	(0.155, 0.059)/ (0.214, 0.275)	8240
3g	352/362	3.02/2.80	417, 434/ 455	1.05/ 0.06, 1.51, 9.74	73/16	68/91	(0.156, 0.062)/ (0.173, 0.179)	3893
3h	349/355	3.01/2.78	417, 432/ 463	0.89/ 0.55, 3.08, 10.6	88/12	63/106	(0.155, 0.065)/ (0.186, 0.222)	6229
3i	357/362	3.01/2.79	416, 434/ 469	0.95/ 0.05, 1.03, 6.37	72/5	66/98	(0.155, 0.059)/ (0.179, 0.233)	8511
3j	355/367	2.96/2.76	418, 434/ 471	0.95/ 0.03, 1.63, 9.19	74/6	64/105	(0.156, 0.060)/ (0.187, 0.245)	8146

Absorbance and emission, photoluminescence quantum yield (PLQY), full width at half maximum (FWHM), life time decay (τ), color coordinates (CIE 1931)

Vibronically structured PL spectra were recorded for the toluene solution of the compounds (Figure 1a). These PL spectra corresponded to pure deep-blue color with CIE1931 color coordinates of ($x < 0.16$, $y < 0.07$) and full width at half maximum (FWHM) < 77 nm (Table 1). Interestingly, FWHM of toluene solutions of substituted compounds **3b-j** was lower in comparison to FWHM of 77 nm observed for the solution of non-substituted compound **3a**. The shapes of PL spectra were similar to the shape of PL spectrum of DMF solution of PI.^[35] PL spectra of the solutions of **3a-j** in toluene were red-shifted in comparison to PL spectrum of the solution of PI. Further, red-shift of emission band of compounds **3a-j** was observed for the solution in chloroform, THF, and acetone, owing to an increase in the polarity of the solvents (Figure S2).

As a result, different variations of Stokes shifts ($\Delta U = U_{abs} - U_{em}$) displaying positive solvatochromism and consistently proving CT character of their emission (Table 1) were obtained for the studied compounds. Non-structured PL spectra of the polar chloroform, THF, and acetone solutions of compounds **3a-j** support the presumption that emission is a result of recombination of CT excited states. To investigate the effect of the substitution pattern of the derivatives THDP and PI derivatives on their

emission behavior, the dependence of their Stokes shifts versus orientation polarizability of the chosen solvents (Δf) were linearly fitted (Figure 1d). The different slopes (ranging from 2633 to 8511 cm⁻¹) of these linear dependencies demonstrated differences in dipole moments of excited singlet states of compounds **3a-j** according to the Lippert-Mataga law (Table 1).^[36] Different electron-donating or electron-accepting substituents of phenyl group attached to PI moiety resulted in slightly different ICT behavior of compounds **3a-j**. Because of relatively low Lippert-Mataga slopes for compounds **3a-j**, some contribution of recombination of locally-excited states to their emission is possible. Non-structured nature of PL spectra of THF solutions of compounds **3a-j** at 77 K also suggests ICT emission (Figure 2). At 77 K, phosphorescence was not detected apparently due to the presence of bulky BTHDP unit. Broadening of PL spectra of the films of **3a-j** corresponds to some loss in deep-blue color purity in comparison to that of toluene solutions (Figure 1b). FWHM lower than 137 nm and CIE 1931 color coordinates of ($x < 0.16$, $y < 0.07$) were obtained for PL of **3a-j** in solid-state (Table 2). Nevertheless, more than twice the higher PLQY of compound **3f** containing appropriate substituent in comparison to PLQY of non-substituted counterpart **3a** demonstrated efficiency of post-functionalization in increase of potential for OLED applications.

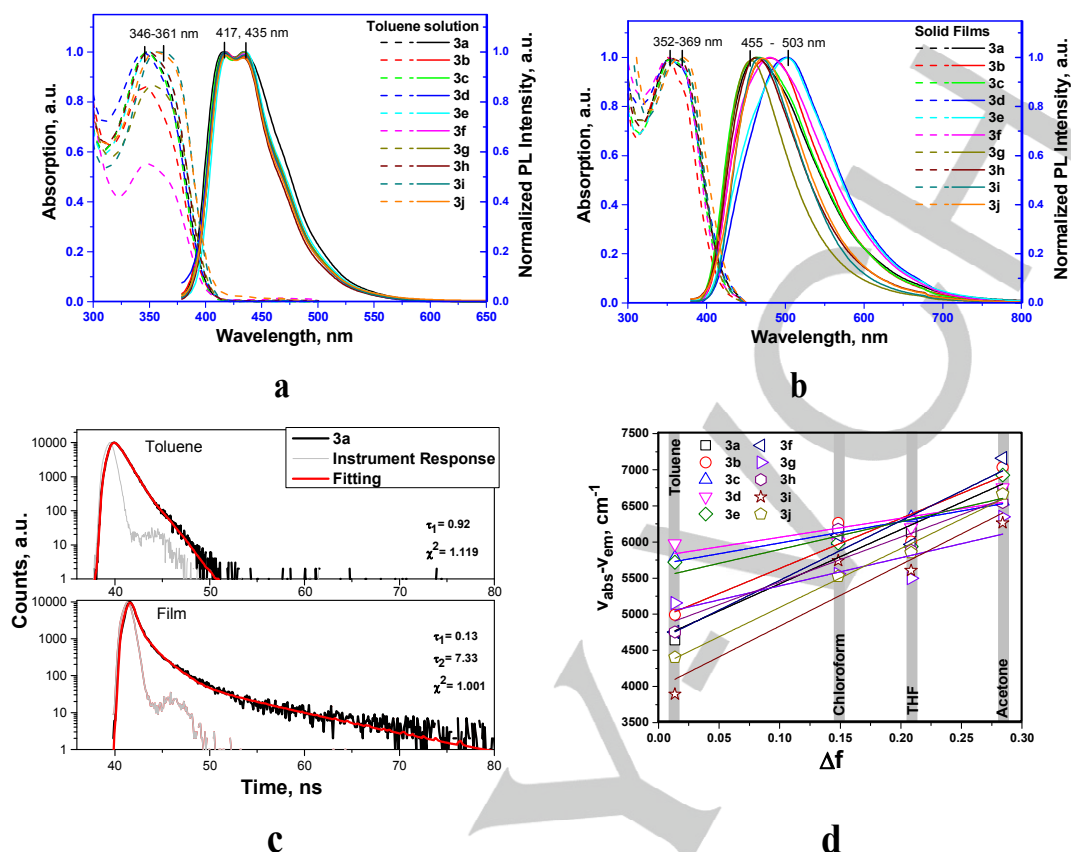


Figure 1 Absorption (dashed lines), and PL spectra (solid lines) of the solutions of compounds 3a-j in toluene (a) and of solid-state samples (b); PL decays of toluene solution and solid film of compound 3a (c) and Lippert-Mataga plots displaying correlation between orientation polarizability of the solvent (Δf) and the Stokes shifts ($\Delta\nu = \nu_{\text{abs}} - \nu_{\text{em}}$) for compounds 3a-j (d)

Thermal, electrochemical and photoelectrical characterization

Most of the synthesized compounds, except **3i**, were obtained after purification as crystalline or semi-crystalline substances, as confirmed by differential scanning calorimetry (DSC) measurements. Their melting temperatures (T_m) ranged from 240 to 379 °C. All the compounds were found to be capable of glass formation. They showed relatively high glass transition temperatures (T_g) of 176-205 °C (Figure S6, Table 2). Such high

T_g values can apparently be explained by relatively high molecular weights and the rigid structures of the compounds. Small differences in T_g values of compounds **3a-j** can be attributed either to their different molecular weights or to different intermolecular interactions in solid states determined by different substituents of PI moiety.

To estimate energy levels of compounds **3a-j**, at the preliminary stage, cyclic voltammograms (CV) of their solutions were recorded (Figure 2a). The reversible oxidations and reductions were observed, which highlighted their good electrochemical stability of the compounds. Since all the studied compounds contain THDP and PI moieties, the similar values of oxidation and

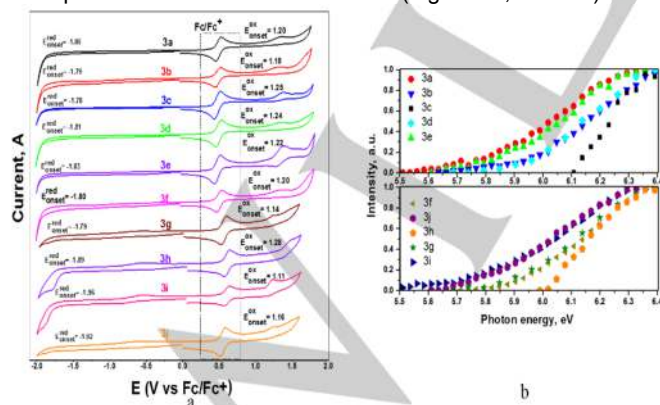
FULL PAPER

Table 2 Thermal, electrochemical, electro optical and charge-transporting characteristics of compounds 3a-j

Compounds	T_g , °C	T_m , °C	I_p^{CV}/I_p^{PE} , eV	E_A^{CV}/E_A^{PE} , eV	μ_h^a , cm ² /Vs
3a	185	348	6/5.74	2.94/2.71	$5.8 \cdot 10^{-6}$
3b	179	341	5.98/5.90	3.01/2.89	-
3c	184	379	6.05/6.11	3.02/3.06	$9 \cdot 10^{-6}$
3d	176	362	6.04/5.92	2.99/2.9	-
3e	189	324	6.02/5.81	2.97/2.8	-
3f	197	373	6/5.92	3/2.9	$2.4 \cdot 10^{-6}$
3g	207	337	5.94/5.88	3.01/2.86	-
3h	176	286	6.08/5.99	2.91/2.98	$3.7 \cdot 10^{-6}$
3i	205	-	5.91/5.77	2.84/2.76	-
3j	198	240	5.96/5.75	2.88/2.79	-

^a $I_p^{PCV} = 4.8 + E_{ox,onset}$; ^b $E_{ACV} = 4.8 - E_{red,onset}$; a taken at electric field of $6.4 \cdot 10^5$ V/cm.

reduction potentials were obtained. Small differences were determined by the different substituents with weak electron-accepting or electron-donating abilities attached to PI moiety (Figure 2a). Oxidation of THDP moiety and reduction of PI moiety were responsible for observed oxidation and reduction peaks of compounds **3a-j**. Ionization potential (I_p^{CV}) and electron affinity (E_A^{CV}) values estimated from CV measurements were obtained in the ranges of 5.91-6.05 and 2.97-3.07 eV, respectively (Table 2). Since I_p^{CV} and E_A^{CV} energy levels are not directly related to the solid layers of organic semiconductors, vacuum-deposited films of **3a-j** were additionally tested by electron photoemission spectrometry in air (PES). The values of ionization potentials (I_p^{PES}) for **3a-j** in the condensed phase were estimated from the corresponding photoelectron emission spectra extrapolating their linear parts to zero of the ordinate axes (Figure 2b, Table 2).

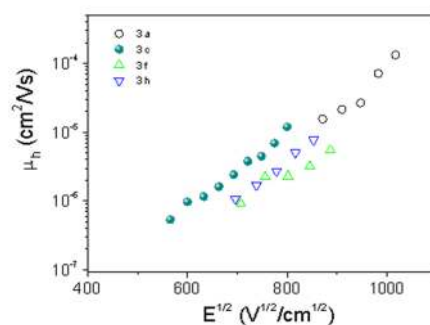
**Figure 2** (a) Cyclic voltammograms of the solutions and (b) photoelectron emission spectra of vacuum-deposited films of compounds 3a-j

Meanwhile, electron affinities (E_A^{PES}) were calculated using the equation $E_A = I_p^{PES} - E_g$, where E_g is optical band-gap energy obtained

from the low-energy edge of absorption spectra of vacuum-deposited films of **3a-j** (Figure 3b, Table 2). Showing the similar trends, I_p^{PES} and E_A^{PES} values of compounds **3a-j** were slightly different from the corresponding I_p^{CV} and E_A^{CV} values (Table 2). The values of I_p^{PES} and E_A^{PES} of compounds **3a-j** were in good agreement with the corresponding energy levels of functional materials of OLEDs and efficient charge injection from the electrodes can be predicted.

Charge-transporting properties

Owing to donor-acceptor molecular structures of the studied PI and phenanthridine derivatives, we expected bipolar charge-transporting properties. Such expectations were partly grounded on the previously published phenanthridine/phenanthroimidazole based compounds which showed relatively good hole or electron-transporting properties.^[37-38] To verify these expectations, time-of-flight (TOF) technique was used for testing diode-like samples with the structure of ITO/vacuum-deposited film/aluminum. Unsubstituted compound **3a** showed hole mobility of $1.3 \cdot 10^{-4}$ cm²/V at electric fields higher than 10^6 V/cm (Figure 3). Post functionalized compounds **3c**, **3f** and **3h** showed hole mobilities similar to those of compound **3a** at the same electric field. This result indicated the absence of significant effects of post functionalization on hole mobility's of the studied derivatives. The tested compounds were characterized by dispersive hole transport, as was evident from the shapes of their photocurrent transients (Figure S7). It was not possible to obtain transit times (required for calculations of charge mobility) from photocurrent transients for the other compounds, apparently due to the strong charge-transport dispersing which is typical for good emitters.^[39] For the same reasons, transit times for electrons were also not detected in the corresponding photocurrent transients.

**Figure 3** Electric field dependences of the hole mobility in vacuum-deposited film of compounds 3a, 3c, 3f and 3h

Electroluminescence

Taking into account that compounds **3a**, **3c**, **3f** and **3h** are characterized by relatively high PLQYs in solid-state and that they are capable of transporting charges, electroluminescent properties of the non-doped light-emitting layers of these selected

FULL PAPER

compounds were further tested in OLEDs with the structure ITO/MoO₃(1 nm)/NPB (30 nm)/**3a**, **3c**, **3f** or **3h** (18 nm)/BPhen (33 nm)/LiF(0.5 nm)/Al. The layers of molybdenum trioxide (MoO₃) and lithium fluoride (LiF) were used as hole- and electron-injection layers, and the layers of N,N'-di(1-naphthyl)-N,N'-diphenyl-(1,1'-biphenyl)-4,4'-diamine (NPB) and bathophenanthroline (BPhen) were employed as hole- and electron-transporting layers, respectively. As a result, energy barriers which might prevent charge-injection into the light-emitting layers were absent in the designed OLED structures (Figure 4a). In addition, the layers of NPB and BPhen acted as electron- and hole-blocking layers due to the LUMO-LUMO energy barrier between NPB and light-emitting layers and the HOMO-HOMO energy barrier between BPhen and light-emitting layers, respectively (Figure 4a). Thus, recombination of charge pairs was anticipated within the light-emitting layers of **3a**, **3c**, **3f** or **3h**. This expectation was in good agreement with EL spectra of OLEDs based on **3a**, **3c**, **3f** or **3h** (Figure 4b). The similar EL spectra with the intensity maxima at 474 nm were observed for all the fabricated devices. Stable EL spectra under different electrical excitations were observed for the devices, showing that the recombination zone was not shifted to the charge-transporting layers under high electric fields partly due to the good charge-blocking properties of NPB and BPhen (Figure S6). EL spectra of devices **3a**, **3c**, **3f** and **3h**, being only slightly different due to the different excitations used, i.e. optical and electrical (Figure 1b, 4b), were in good agreement with PL spectra of the corresponding films. CIE coordinates of the fabricated devices corresponded with blue color (Figure S9, Table 3).

By tenfold increase in maximum brightness was observed for the device, based on compound **3f** containing OCH₃ group in comparison to that of device based on non-substituted emitter **3a** (Figure 4c). To understand why tenfold increase in maximum brightness was observed for the device, based on compound **3f** containing methoxy group in comparison to that of device based on non-substituted emitter **3a** (Figure 4c), we plotted brightness versus current density for the fabricated devices (Figure S10). These dependences were well linearly fitted with the slope of 1 for all the devices at low brightness demonstrating that their electroluminescence resulted from singlet exciton recombination.^[40] In case of device **f**, the linear dependence of brightness versus current density was observed at high current density (Figure R1). This observation can be explained by the perfect charge balance and/or negligible quenching of excitons at broad range of electric fields in light emitting layer **3f**. In contrast, brightness of device **a** based on light-emitting layer **3a** is apparently limited by charge disbalance and/or exciton quenching at high electric fields (Figure S10).

In contrast to high roll-off efficiency of blue phosphorescent OLEDs which suffered from formation of "hot excitons" due to the presence of long-lived triplet excitons,^[41] the fabricated blue fluorescent device **3f** showed low roll-off efficiency (Figure 4d). Its external quantum efficiency (EQE) at very high brightness (L) of 10000 cd/m² for blue OLEDs exhibited a slight drop in comparison to its maximum EQE of 1.6% (Figure 4d). Better OLED performances of devices based on **3c** and **3f**, in comparison with that of the device based on **3a**, were mainly related to higher PLQY values of the films of **3c** and **3f** in comparison with that of

the film of **3a**. In addition, differences between charge-injection and charge-transporting properties of compounds **3a**, **3c**, **3f** and **3h** should also play important roles. The differences between current density versus applied voltages characteristics were observed for the studied devices (Figure 4c). Slightly different turn-on voltages (V_{on} = 4.9–5.4 V) were obtained for the fabricated devices (Table 3). For the device based on **3f**, the film of which showed PLQY of 59%, maximum EQE was two times lower than its theoretical maximum (4.4%) estimated according to the well-known relationship $\eta_{ext} = (\gamma \times \eta_{ST} \times PLQY) \times \eta_{out}$ using the charge balance factor $\gamma = 1$ and the fraction of radiative excitons $\eta_{ST} = 0.25$ for simple fluorescent emitters.^[41] Therefore, further improvement of EQE of device based on **3f** can be expected. Nevertheless, the performed electroluminescent investigations not only testify the potential of the derivatives of THDP and PI in blue fluorescent OLEDs, but also demonstrate the requirements of their modifications through smart molecule design.

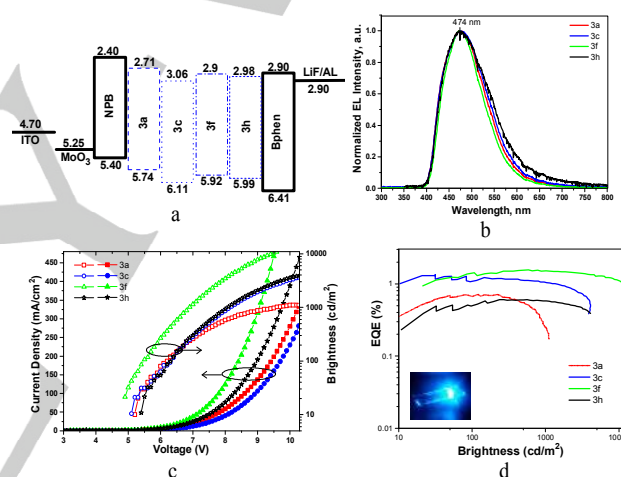


Figure 4 Equilibrium energy diagram (a), EL spectra recorded at 7 V (b), characteristics of current density and brightness versus applied voltages (c) and dependences of EQEs versus brightness (d) of OLEDs. The inset is photo of device **3f**

Theoretical Calculations

To estimate the differences between the geometric and optical properties, quantum-chemical calculations were performed by density functional theory (DFT) and time-dependent density functional theory (TD-DFT) at the B3LYP/6-31G(d) level. The calculated highest occupied molecular orbital (HOMO), lowest unoccupied molecular orbital (LUMO), oscillator strength (f), excited state energies and DEST are depicted in Figure S1 and Table S2. The HOMO was mainly localized in PI units and extended to phenyl parts of BTHDP core, there by suggesting that PI acts as an acceptor. The LUMO was fully occupied on the BTHDP donor unit and partially extended to the imidazole parts of PI units, which suggested that the nature of the substitution could also influence the optical properties.

FULL PAPER

Table 3 Fabricated OLED device for **3a**, **3c**, **3f** and **3h**

Device	V _{on} (V)	L _{max} (cd/m ²)	L at 9 V (cd/m ²)	PE _{max} (lm/W)	CE _{max} (cd/A)	EQ _{Emax} (%)	CIE1931 coordinates (x, y) at 10V
3a: ITO/MoO ₃ /NPB/3a/TPBi/LiF/Al	5.2	1100	900	0.8	1.9	0.8	(0.194, 0.256)
3c: ITO/MoO ₃ /NPB/3c/TPBi/LiF/Al	5.1	4100	2100	1.2	1.9	1.2	(0.185, 0.244)
3f: ITO/MoO ₃ /NPB/3f/TPBi/LiF/Al	4.9	11300	8300	1.6	1.9	1.6	(0.179, 0.246)
3h: ITO/MoO ₃ /NPB/3h/TPBi/LiF/Al	5.4	4100	2200	0.6	0.7	0.6	(0.201, 0.267)

PE_{max} and CE_{max} are maximum power and current efficiencies, respectively

For example, a slightly distinct trend was observed in **3g** and **3i**; LUMO was fully localized only on N-phenyl parts of PI core owing to the strong CN and NO₂ acceptors at the para position. Due to this, the HOMO was completely isolated and widely distributed to PI, and the THDP core resulted in a small overlap of HOMO and LUMO. This led to a small calculate lowest singlet-triplet gap (ΔE_{ST}) values of 0.33 and 0.03 eV, oscillator strength (*f*) values of 0.034 and 0.008 for **3g** and **3i** respectively. Hence, the increased charge transfer (CT) character with red-shifted properties can be observed. While the other emitters displayed almost similar singlet and triplet energies, large ΔE_{ST} and increased *f*, with completely overlapped HOMO and LUMO levels, suggest a probable increase in PLQYs. Furthermore, the calculated HOMO levels were in the range of 5.03-5.18 eV, while the LUMO levels were in the range of 1.42-1.50 eV, which gave almost similar energy gap (*E_g*) of 3.60 eV. Deeper HOMO values of -5.30, -5.33 eV and LUMO values of -1.94, -2.77 eV were observed for **3g** and **3i** respectively due to the acceptor's strength of CN and NO₂ functionalities. The calculated optical parameters are tabulate in Table S2.

Conclusions

Ten new fluorescent derivatives of tetrahydrodibenzophenanthridine and phenanthroimidazole were designed, synthesized and characterized as emitters for blue organic light-emitting diodes. Toluene solutions of the compounds exhibited a high photoluminescence quantum yield up to 93 %. For the films, photoluminescence quantum yields up to 59% were observed. The best blue OLED exhibited brightness exceeding 10000 cd/m² and a relatively low roll-off efficiency. The best photoluminescence and electroluminescence performances were observed for the compound containing methoxy substituents. We performed DFT calculations and observed the lowest singlet-triplet gap (ΔE_{ST}) values of 0.33 and 0.03 eV, oscillator strength (*f*) values of 0.034 and 0.008 for CN and NO₂ derivatives. Interestingly, the compound **3g** and **3i** values were HOMO levels, and they were in the range of 5.03-5.18 eV, while the LUMO levels were in the range of 1.42-1.50 eV, which offered an almost similar energy gap *E_g* of 3.60 eV. The deeper HOMO values were found to be -5.30, -5.33 eV while the LUMO values were -1.94, -2.77 eV.

Experimental section

General information: All organic chemicals and solvents were purchased from Sigma-Aldrich, TCI, SD Fine, and AVRA and were used without further purification. NMR spectra were taken on Bruker 400 MHz using CDCl₃ as the solvent with tetramethylsilane as an internal standard. Melting points were measured on a microprocessor-based melting point apparatus and were not corrected. HRMS values were obtained on a Jeol

GC Mate II GC-mass spectrometer. FTIR spectra of the synthesized organic compounds were recorded using a Jasco-4100 spectrometer instrument. Ultraviolet-visible spectra were recorded using a Hitachi U-2910 spectrophotometer. Fluorescence spectra in solution and solid state were measured using a Hitachi F7000 fluorescence spectrometer.

Photoluminescence (PL) spectra of 10⁻⁵ M solutions and of solid films of the compounds were recorded using Edinburgh Instrument FLS980 Fluorescence Spectrometer. For recording the UV/VIS and PL spectra, thin solid films were prepared by the spin-coating technique utilizing SPS-Europe Spin150 Spin processor using 1 mg/mL solutions of the compounds in chloroform on the pre-cleaned quartz substrates. The PL spectra were recorded at a low temperature (77 K). Fluorescence quantum yields (Φ_{F1}) of the solutions and of the solid films were estimated using an integrated sphere. Edinburgh Instruments FLS980 spectrometer with Pico Quant LDH-D-C-375 laser (wavelength 374 nm) as the excitation source was utilized for photoluminescence decay curves. Differential scanning calorimetry (DSC) measurements were carried out in a nitrogen atmosphere with a DSC TA Instruments Q2000 thermal analyser at a heating rate of 10 °C/min. The sample (approximately 2-3 mg) was placed in a closed aluminum pan. An empty pan was used as a reference. Electrochemical measurements were performed with an Autolab M101 potentiostat. Standard, three electrode setup consisting of platinum wire working electrode, platinum wire counter electrode and silver wire quasi-reference electrode calibrated vs. ferrocene/ferrocenium redox couple prior to each experiment was used. All electrochemical experiments were

FULL PAPER

conducted in electrolyte: 0.1 M solution of Tetrabutylammoniumhexafluorophosphate (Bu4NPF6) (TCl) in dichloromethane (Chromasolv, HPLC grade). Solutions were degassed with argon prior to experiments and kept in an inert atmosphere during measurements. Onset of oxidation was used for calculation of ionization potential (IP^{CV}) of compounds. While, onset of reduction was used for calculation of electron affinity (EA^{CV}) of compounds. The ionization potential (Ip^{PE}) of the solid state sample was measured by photoelectron emission spectrometry in air as described before in Ref [2]. Indium tin oxide (ITO)/thick layer of compounds/Al were fabricated by depositing organic layers under vacuum of 2×10^{-6} mBar. The charge carrier mobility (μ) measurements of vacuum deposited layer were carried out by the time of flight method (TOF). The TOF experimental setup consisted of a pulsed Nd:YAG laser (EKSPALA NL300, a wavelength of 355 nm, pulse duration 3–6 ns), a Keithley 6517B electrometer, a Tektronix TDS 3052C oscilloscope, and was as described. The transit time (t_{tr}) with the applied bias (V) indicated the passage of charges through the entire thickness (d) of the samples. Hole mobility was calculated as $\mu = d^2/U \cdot t_{tr}$. OLEDs were prepared by vacuum deposition of organic and metal layers onto pre-cleaned ITO coated glass substrate under pressure lower than 2×10^{-6} mBar. Keithley 6517B electrometer, calibrated photodiode and Keithley 2400C source meter were used for recording current density via voltage and luminance via voltage characteristics.

Synthesis of 5-(4-(4,4,5,5-tetramethyl-1,3,2-dioxaborolan-2-yl)phenyl)-7,8,13,14-tetrahydrobenzo[a,i]phenanthridine (1)

A mixture of 4-(4,4,5,5-tetramethyl-1,3,2-dioxaborolan-2-yl)benzaldehyde (10 mmol) and ammonium acetate (15 mmol) was taken in a 100 mL conical flask containing 10 mL absolute ethanol at room temperature, sealed and warmed using water bath 15 min until the dissolution of the solid contents. After bringing the reaction mixture to room temperature, 2-teralone (20 mmol) was added, sealed and the mixture was warmed for 5 min and the reaction mixture was kept aside for 24 h in an open air. After the completion of the reaction was monitored by TLC. The resulting product was purified by the column chromatography over silica gel (60-120 mesh) using n-hexane and ethyl acetate mixture (9:1) as eluent to give the compound (1). Thus obtained solid was further purified by recrystallizing in 1:1 ethanol and tetrahydrofuran mixture to afford compound (1) 65% as a yellow solid.⁴²

Synthesis of 2-(4-Bromophenyl)-1-phenyl-1H-phenanthro-[9,10-d]imidazole (PI) and their derivatives (2a-j)

A mixture of 9, 10-phenanthrenequinone (10.0 mmol), aniline derivatives (10.0 mmol), 4-Bromobenzaldehyde (10.0 mmol), ammonium acetate (15.0 mmol), and acetic acid (15 mL) was

refluxed for 24 hrs. After that, the mixture was cooled to room temperature, and then the crude product was extract with ethyl acetate (3X30 mL) and finally dried with sodium sulfate. It was then purified by chromatography using Hexane/Ethyl acetate (9:1) as an eluent to obtain the product as white powder (2a-j). The characterization of compounds 2a-j were matched with previous reported work.⁴³ Quantitative yield: 75-90%.

Synthesis of 5-(4'-(1-phenyl-1H-phenanthro[9,10-d]imidazol-2-yl)-[1,1'-biphenyl]-4-yl)-7,8,13,14-tetrahydrobenzo[a,i]phenanthridine and their derivatives (3a-j)

A mixture of compound 1 (0.250 g, 6.2 mmol), compound 2a-j (6.82 mmol), Pd(PPh₃)₄ (72 mg, 0.062 mmol) and Cs₂CO₃ (0.404 g, 12.4 mmol) in dioxane/H₂O (4:1) 5 mL was stirred under nitrogen at 80 °C for 24 h. After cooling to room temperature, the reaction mixture was extracted with dichloromethane, and the mixture was further purified by column chromatography (8:2) to obtain a yellow solid 3a-j (Yield: 60-78%).⁴⁴

Synthesis of 5-(4-(4,4,5,5-tetramethyl-1,3,2-dioxaborolan-2-yl)phenyl)-7,8,13,14-tetrahydrobenzo[a,i]phenanthridine (1)

Yellow solid; (Yield 62%); Melting point: 302-304 °C; FTIR (KBr cm⁻¹): 3323, 3070, 2966, 2839, 1606, 1548, 1483, 1425, 1402, 1342, 1259, 1165, 1103, 1043, 1016, 945, 891, 840, 804, 740; ¹H NMR (400 MHz, CDCl₃)TM ppm: 1.36 (s, 12H, CH₂), 2.78 – 2.75 (t, 2H, J=8Hz, CH₂), 2.96 – 2.93 (m, 2H, CH₂), 3.15 – 3.06 (m, 4H, CH₂), 6.88 – 6.87 (d, 2H, J=4Hz, ArCH), 7.12 – 7.08 (m, 1H, ArCH), 7.35 – 7.22 (m, 4H, ArCH), 7.46 – 7.44 (d, 2H, J=8Hz, ArCH), 7.51 – 7.49 (d, 1H, J=8Hz, ArCH), 7.78 – 7.76 (d, 2H, J=8Hz, ArCH), ¹³C NMR {¹H} (100 MHz, CDCl₃)TM ppm: 24.9 (6XCH), 29.2 (CH), 29.4 (CH), 29.5 (CH), 30.9 (CH), 33.1 (CH), 83.8 (C), 125.8 (C), 126.0 (C), 126.8 (C), 127.0 (C), 127.5 (C), 127.6 (C), 127.8 (C), 128.7 (C), 128.9 (C), 129.2 (C), 129.4 (C), 129.7 (C), 132.8 (C), 133.0 (C), 134.7 (C), 138.6 (C), 139.7 (C), 144.8 (C), 145.6 (C), 153.7 (C), 158.1 (C); HRMS (EI-ion trap) for C₃₃H₃₂BNO₂ Calculated [M⁺] m/z 485.2526, Observed Mass: 485.2523.

5-(4'-(1-phenyl-1H-phenanthro[9,10-d]imidazol-2-yl)-[1,1'-biphenyl]-4-yl)-7,8,13,14-tetrahydrobenzo[a,i]phenanthridine(3a)

Yellow solid; (Yield 78%); Melting point: 336-338 °C; FTIR (KBr cm⁻¹): 2935, 2845, 1548, 1452, 1392, 1234, 1145, 1001, 941, 827, 746, 698, 617; ¹H NMR (400 MHz, CDCl₃)TM ppm: 2.81 – 2.78 (t, 2H, J= 6.8Hz, CH₂), 2.98 – 2.95 (t, 2H, J= 8 Hz, CH₂), 3.17 – 3.09 (m, 4H, CH₂), 6.93 – 6.90 (t, 1H, J= 8 Hz, ArCH), 7.00 – 6.98 (d, 1H, J= 8 Hz, ArCH), 7.16 – 7.12 (t, 1H, J= 8 Hz, ArCH), 7.20 –

FULL PAPER

7.18 (d, 1H, J = 8 Hz, ArCH), 7.37 – 7.25 (m, 7H, ArCH), 7.58 – 7.49 (m, 10H, ArCH), 7.67 – 7.63 (t, 6H, J = 8 Hz, ArCH), 7.77 – 7.73 (t, 1H, J = 8 Hz, ArCH), 8.72 – 8.70 (d, 1H, J = 8 Hz, ArCH), 8.79 – 8.76 (d, 1H, J = 8 Hz, ArCH), 8.91 – 8.89 (d, 1H, J = 8 Hz, ArCH); ^{13}C NMR $\{^1\text{H}\}$ (400 MHz, CDCl_3)TM ppm: 29.2 (CH), 29.4 (CH), 29.5 (CH), 33.1 (CH), 120.8 (C), 122.8 (C), 123.0 (C), 123.1 (C), 124.1 (C), 124.8 (C), 125.6 (C), 125.7 (C), 126.1 (C), 126.2 (C), 126.7 (4XC), 126.9 (C), 127.1 (C), 127.2 (C), 127.3 (C), 127.5 (4XC), 127.7 (C), 127.8 (C), 128.2 (C), 128.7 (C), 128.9 (4XC), 129.1 (C), 129.3 (C), 129.4 (C), 129.6 (2XC), 129.8 (C), 130.2 (2XC), 130.3 (C), 137.5 (C), 138.7 (C), 138.8 (C), 139.5 (C), 139.6 (C), 141.0 (C), 141.3 (C), 145.8 (C), 150.6 (C), 153.3 (C), 158.2 (C); HRMS (EI-ion trap) for $\text{C}_{54}\text{H}_{37}\text{N}_3$ Calculated $[\text{M}^+]$ m/z: 727.2987, Observed Mass: 727.2985.

5-(4'-(1-(p-tolyl)-1H-phenanthro[9,10-d]imidazol-2-yl)-[1,1'-biphenyl]-4-yl)-7,8,13,14-tetrahydrodibenzo[a,i]phenanthridine(3b)

Yellow solid; (Yield 74%); Melting point: 308-310 °C; FTIR (KBr cm^{-1}): 3032, 2954, 2926, 2845, 1776, 1608, 1518, 1452, 1390, 1232, 1159, 1033, 950, 825, 748, 721, 619; ^1H NMR (400 MHz, CDCl_3)TM ppm: 2.55 (s, 3H, CH_3), 2.80 – 2.79 (m, 2H, CH_2), 2.98 – 2.94 (m, 2H, CH_2), 3.17-3.09 (m, 4H, CH_2), 7.05 – 6.89 (m, 2H, ArCH), 7.17 – 7.12 (m, 1H, ArCH), 7.45 – 7.22 (m, 12H, ArCH), 7.62- 7.49 (m, 9H, ArCH), 7.69 – 7.65 (t, 2H, J = 8 Hz, ArCH), 7.76 – 7.72 (t, 1H, J = 8 Hz, ArCH), 8.71 – 8.69 (d, 1H, J = 8 Hz, ArCH), 8.77 – 8.75 (d, 1H, J = 8 Hz, ArCH), 8.90 – 8.88 (d, 1H, J = 8 Hz, ArCH); ^{13}C NMR $\{^1\text{H}\}$ (400 MHz, CDCl_3)TM ppm: 21.5 (CH), 29.2 (CH), 29.4 (CH), 29.5 (CH), 33.1 (CH), 119.9 (C), 120.9 (C), 122.7 (C), 123.1 (C), 124.0 (C), 124.8 (C), 125.5 (C), 125.7 (C), 125.8 (C), 126.0 (C), 126.2 (C), 126.7 (2XC), 126.9 (C), 127.0 (C), 127.0 (C), 127.2 (C), 127.6 (2XC), 127.7 (C), 127.8 (C), 128.2 (C), 128.3 (2xC), 128.7 (C), 128.8 (C), 128.9 (C), 129.2 (2XC), 129.5 (C), 129.6 (2XC), 130.2 (C), 130.3 (C), 130.8 (C), 132.9 (C), 133.0 (C), 136.1 (C), 137.4 (C), 138.7 (C), 139.5 (C), 139.6 (C), 139.9 (C), 140.1 (C), 141.9 (C), 141.3 (C), 145.8 (C), 150.6 (C), 153.3 (C), 158.2 (C); HRMS (EI-ion trap) for $\text{C}_{55}\text{H}_{39}\text{N}_3$ Calculated $[\text{M}^+]$ m/z: 741.3144, Observed Mass: 741.3141.

5-(4'-(1-(4-fluorophenyl)-1H-phenanthro[9,10-d]imidazol-2-yl)-[1,1'-biphenyl]-4-yl)-7,8,13,14-tetrahydrodibenzo[a,i]phenanthridine(3c)

Yellow solid; (Yield 69%); Melting point: 354-356 °C; FTIR (KBr cm^{-1}): 3061, 2954, 2837, 1508, 1450, 1388, 1219, 1149, 1001, 948, 831, 748, 723, 667, 617; ^1H NMR (400 MHz, CDCl_3)TM ppm: 2.81 – 2.78 (t, 2H, J = 8 Hz, CH_2), 2.98 – 2.94 (m, 2H, CH_2), 3.17 – 3.09 (m, 4H, CH_2), 6.93 – 6.90 (t, 1H, J = 8 Hz, ArCH), 7.00 – 6.98 (d, 1H, J = 8 Hz, ArCH), 7.16 – 7.12 (t, 1H, J = 8 Hz, ArCH), 7.21 – 7.19 (d, 1H, J = 8 Hz, ArCH), 7.27 – 7.25 (d, 2H, J = 8 Hz, ArCH), 7.37 – 7.29 (m, 7H, ArCH), 7.59 – 7.51 (m, 10H, ArCH), 7.68 – 7.63 (m, 3H, ArCH), 7.77 – 7.73 (t, 1H, J = 8 Hz, ArCH), 8.72 – 8.70 (d, 1H, J = 8 Hz, ArCH), 8.79 – 8.77 (d, 1H, J = 8 Hz,

ArCH), 8.89 – 8.87 (d, 1H, J = 8 Hz, ArCH); ^{13}C NMR $\{^1\text{H}\}$ (400 MHz, CDCl_3)TM ppm: 29.2 (CH), 29.4 (CH), 29.5 (CH), 33.1 (CH), 117.2 (C), 117.4 (C), 120.6 (C), 122.8 (C), 122.9 (C), 123.1 (C), 124.2 (C), 125.0 (C), 125.7 (C), 126.0 (C), 126.3 (C), 126.8 (C), 126.9 (4xC), 127.1 (C), 127.1 (C), 127.3 (C), 127.6 (C), 127.7 (4XC), 127.9 (C), 128.2 (C), 128.3 (C), 128.7 (C), 128.9 (4XC), 129.1 (C), 129.3 (C), 129.7 (C), 130.4 (C), 130.9 (C), 131.0 (C), 132.9 (C), 133.0 (C), 134.8 (C), 137.5 (C), 138.7 (C), 139.4 (C), 139.7 (C), 141.2 (C), 141.5 (C), 145.8 (C), 150.76 (C), 153.2 (C), 158.2 (C); HRMS (EI-ion trap) for $\text{C}_{54}\text{H}_{36}\text{FN}_3$ Calculated $[\text{M}^+]$ m/z: 745.2893, Observed Mass: 745.2890.

5-(4'-(1-(4-chlorophenyl)-1H-phenanthro[9,10-d]imidazol-2-yl)-[1,1'-biphenyl]-4-yl)-7,8,13,14-tetrahydrodibenzo[a,i]phenanthridine(3d)

Yellow solid; (Yield 64%); Melting point: 330-332 °C; FTIR (KBr cm^{-1}): 3059, 2945, 2845, 1608, 1492, 1396, 1271, 1232, 1166, 1002, 948, 833, 748, 696, 617; ^1H NMR (400 MHz, CDCl_3)TM ppm: 2.81 – 2.73 (m, 2H, CH_2), 2.98-2.93 (m, 2H, CH_2), 3.17 – 3.08 (m, 4H, CH_2), 6.70 – 6.68 (d, 1H, J = 8 Hz, ArCH), 7.00 – 6.87 (m, 4H, ArCH), 7.16 – 7.08 (m, 1H, ArCH), 7.37- 7.21 (m, 2H, ArCH), 7.68 – 7.49 (m, 10H, ArCH), 7.77-7.73 (t, 1H, J = 8 Hz, ArCH), 8.89 – 8.70 (m, 2H, ArCH); ^{13}C NMR $\{^1\text{H}\}$ (400 MHz, CDCl_3)TM ppm: 29.2 (CH), 29.4 (CH), 29.5 (CH), 30.9 (CH), 33.1 (CH), 115.8 (C), 120.6 (C), 122.8 (C), 123.1 (C), 124.2 (C), 125.0 (C), 125.6 (C), 125.7 (C), 126.0 (C), 126.4 (4XC), 126.8 (C), 126.9 (C), 126.9 (C), 127.1 (C), 127.4 (4XC), 127.6 (C), 127.7 (C), 127.8 (C), 127.9 (C), 128.0 (C), 128.3 (C), 128.7 (4XC), 129.3 (C), 129.5 (C), 129.7 (C), 130.4 (C), 130.4 (C), 130.5 (C), 131.1 (C), 133.0 (C), 135.8 (C), 138.7(C), 139.6 (C), 141.2 (C), 141.4 (C), 145.8 (C), 150.6 (C), 153.2 (C), 157.9 (C), 158.2 (C); HRMS (EI-ion trap) for $\text{C}_{23}\text{H}_{18}\text{ClN}_2$ Calculated $[\text{M}^+]$ m/z: 761.2598, Observed Mass: 761.2591.

5-(4'-(1-(3,5-dimethylphenyl)-1H-phenanthro[9,10-d]imidazol-2-yl)-[1,1'-biphenyl]-4-yl)-7,8,13,14-tetrahydrodibenzo[a,i]phenanthridine(3e)

Yellow solid; (Yield 67%); Melting point: 318-320 °C; FTIR (KBr cm^{-1}): 3018, 2943, 2839, 1608, 1469, 1392, 1145, 1001, 947, 831, 748, 725, 619; ^1H NMR (400 MHz, CDCl_3)TM ppm: 2.43 (s, 6H, CH_3), 2.82 – 2.79 (t, 2H, J = 8 Hz, CH_2), 2.99 – 2.95 (t, 2H, J = 8 Hz, CH_2), 3.18 – 3.10 (m, 4H, CH_2), 6.94 – 6.90 (t, 1H, J = 8 Hz, ArCH), 7.01 – 6.99 (d, 1H, J = 8 Hz, ArCH), 7.22 – 7.13 (m, 5H, ArCH), 7.33 – 7.26 (m, 11H, ArCH), 7.38 – 7.34 (t, 1H, J = 8 Hz, ArCH), 7.54 – 7.50 (m, 5H, ArCH), 7.60 - 7.58 (d, 4H, J = 8 Hz, ArCH), 7.67 – 7.63 (t, 1H, J = 8 Hz, ArCH), 7.75 – 7.73 (d, 3H, J = 8 Hz, ArCH), 8.72 – 8.70 (d, 1H, J = 8 Hz, ArCH), 8.78 – 7.76 (d, 1H, J = 8 Hz, ArCH), 8.90 – 8.88 (d, 2H, J = 8 Hz, ArCH); ^{13}C NMR $\{^1\text{H}\}$ (400 MHz, CDCl_3)TM ppm: 21.1 (CH), 29.2 (CH), 29.5 (CH), 29.6 (CH), 33.3 (2XCH), 115.8 (C), 125.8 (C), 126.0 (C), 126.1 (C), 126.5 (4XC), 126.6 (C), 126.9 (C), 126.9 (C), 127.1 (C), 127.4 (4XC), 127.5 (C), 127.7 (C), 127.9 (C), 128.1 (C), 128.2 (4XC),

FULL PAPER

128.7 (C), 128.9 (C), 129.0 (C), 129.5 (4XC), 129.6 (C), 129.7 (C), 133.0 (C), 133.1 (2XC), 134.6 (C), 137.0 (C), 138.2 (C), 138.7 (C), 138.8 (2XC), 139.6 (C), 139.7 (C), 140.2 (C), 141.2 (C), 145.8 (C), 146.4 (C), 153.4 (C), 158.2 (C); HRMS (EI-ion trap) for $C_{56}H_{41}N_3$ Calculated $[M^+]$ m/z: 755.3300, Observed Mass: 755.3298.

5-(4'-(1-(4-methoxyphenyl)-1H-phenanthro[9,10-d]imidazol-2-yl)-[1,1'-biphenyl]-4-yl)-7,8,13,14-tetrahydrobenzo[a,i]phenanthridine(3f)

Yellow solid; (Yield 66%); Melting point: 358-360 °C; FTIR (KBr cm^{-1}): 2960, 2829, 1608, 1508, 1450, 1394, 1290, 1244, 1166, 1107, 1024, 948, 831, 746, 725, 617; 1H NMR (400 MHz, $CDCl_3$) $^{\text{TM}}$ ppm: 2.82 – 2.78 (t, 2H, J = 8 Hz, CH_2), 2.98 – 2.95 (t, 2H, J = 8 Hz, CH_2), 3.18 – 3.09 (m, 4H, CH_2), 3.97 (s, 3H, OCH_3), 6.94 – 6.90 (t, 1H, J = 8 Hz, ArCH), 7.00 – 6.99 (d, 1H, J = 4 Hz, ArCH), 7.16 – 7.10 (m, 3H, ArCH), 7.38 – 7.26 (m, 14H, ArCH), 7.60 – 7.45 (m, 10H, ArCH), 7.77 – 7.64 (m, 4H, ArCH), 8.72 – 8.70 (d, 1H, J = 8 Hz, ArCH), 8.79 – 8.77 (d, 1H, J = 8 Hz, ArCH), 8.90 – 8.88 (d, 1H, J = 8 Hz, ArCH); ^{13}C NMR $\{^1H\}$ (400 MHz, $CDCl_3$) $^{\text{TM}}$ ppm: 29.2 (CH), 29.5 (CH), 29.6 (CH), 33.1 (CH), 55.4 (2XCH), 114.3 (C), 115.6 (C), 125.7 (C), 125.7 (C), 126.0 (C), 126.6 (C), 126.6 (C), 126.9 (4XC), 127.0 (C), 127.4 (C), 127.6 (4XC), 127.7 (C), 127.8 (C), 128.2 (C), 128.4 (4XC), 128.7 (C), 128.9 (C), 129.6 (C), 129.6 (2XC), 129.7 (C), 129.9 (C), 130.3 (C), 130.7 (2XC), 131.2 (C), 131.3 (C), 132.9 (C), 133.5 (C), 134.5 (C), 138.3 (C), 138.7 (C), 138.7 (C), 139.7 (C), 140.3 (C), 141.2 (C), 145.8 (C), 146.8 (C), 153.4 (C), 158.2 (C), 159.2 (C); HRMS (EI-ion trap) for $C_{55}H_{39}N_3O$ Calculated $[M^+]$ m/z: 757.3093, Observed Mass: 757.3090.

4-(2-(4'-(7,8,13,14-tetrahydrobenzo[a,i]phenanthridin-5-yl)-[1,1'-biphenyl]-4-yl)-1H-phenanthro[9,10-d]imidazol-1-yl)benzotrile(3g)

Yellow solid; (Yield 72%); Melting point: 328-330 °C; FTIR (KBr cm^{-1}): 2978, 1604, 1508, 1452, 1396, 1253, 1166, 1118, 1004, 950, 831, 748, 725, 617; 1H NMR (400 MHz, $CDCl_3$) $^{\text{TM}}$ ppm: 2.81 – 2.78 (t, 2H, J = 8 Hz, CH_2), 2.98 – 2.95 (t, 2H, J = 8 Hz, CH_2), 3.17 – 3.09 (m, 4H, CH_2), 6.94 – 6.90 (t, 1H, J = 8 Hz, ArCH), 7.00 – 6.98 (d, 1H, J = 8 Hz, ArCH), 7.26 – 7.10 (m, 2H, ArCH), 7.37 – 7.25 (m, 7H, ArCH), 7.60 – 7.51 (m, 10H, ArCH), 7.70 – 7.66 (m, 3H, ArCH), 7.78 – 7.74 (t, 1H, J = 8 Hz, ArCH), 7.93 – 7.92 (d, 2H, J = 4 Hz, ArCH), 8.72 – 8.70 (d, 1H, J = 8 Hz, ArCH), 8.80 – 8.78 (d, 1H, J = 8 Hz, ArCH), 8.88-8.86 (d, 1H, J = 8 Hz, ArCH); ^{13}C NMR $\{^1H\}$ (400 MHz, $CDCl_3$) $^{\text{TM}}$ ppm: 29.2 (CH), 29.4 (CH), 29.5 (CH), 33.1 (CH), 113.9 (C), 117.7 (C), 120.4 (C), 122.4 (C), 122.8 (C), 123.1 (C), 124.4 (C), 125.2 (C), 125.7 (C), 126.0 (C), 126.0 (4XC), 126.5 (C), 126.9 (C), 127.0 (C), 127.1 (C), 127.5 (4XC), 127.6 (C), 127.7 (C), 127.9 (C), 128.4 (C), 128.6 (C), 128.7 (4XC), 128.9 (C), 129.4 (C), 129.6 (C), 129.8 (C), 130.2 (C), 130.4 (C), 132.9 (C), 133.0 (C), 134.0 (C), 138.0 (C), 138.7 (C), 139.1 (C),

139.6 (C), 141.6 (C), 142.8 (C), 145.8 (C), 150.5 (C), 153.2 (C), 158.2 (C); HRMS (EI-ion trap) for $C_{55}H_{36}N_4$ Calculated $[M^+]$ m/z: 752.2940, Observed Mass: 752.2938.

5-(4'-(1-(3,5-dimethoxyphenyl)-1H-phenanthro[9,10-d]imidazol-2-yl)-[1,1'-biphenyl]-4-yl)-7,8,13,14-tetrahydrobenzo[a,i]phenanthridine(3h)

Yellow solid; (Yield 60%); Melting point: 278-280 °C; FTIR (KBr cm^{-1}): 2949, 1724, 1593, 1452, 1330, 1236, 1203, 1155, 1041, 999, 945, 831, 746, 725, 617; 1H NMR (400 MHz, $CDCl_3$) $^{\text{TM}}$ ppm: 2.81 – 2.78 (t, 2H, J = 6 Hz, CH_2), 2.98 – 2.95 (t, 2H, J = 6 Hz, CH_2), 3.17 – 3.09 (m, 4H, CH_2), 3.80 (s, 6H, OCH_3), 6.72 – 6.71 (d, 3H, J = 4 Hz, ArCH), 6.94 – 6.90 (t, 1H, J = 8 Hz, ArCH), 7.01 – 6.99 (d, 1H, J = 8 Hz, ArCH), 7.16 – 7.13 (t, 1H, J = 8 Hz, ArCH), 7.37 – 7.25 (m, 9H, ArCH), 7.60 – 7.52 (m, 9H, ArCH), 7.67 – 7.63 (t, 1H, J = 8 Hz, ArCH), 7.78 – 7.72 (m, 3H, ArCH), 8.72 – 8.70 (d, 1H, J = 8 Hz, ArCH), 8.78 – 8.76 (d, 1H, J = 8 Hz, ArCH), 8.89 – 8.87 (d, 1H, J = 8 Hz, ArCH); ^{13}C NMR $\{^1H\}$ (400 MHz, $CDCl_3$) $^{\text{TM}}$ ppm: 29.2 (CH), 29.5 (CH), 29.6 (CH), 33.1 (CH), 55.8 (2XCH), 102.0 (C), 102.3 (C), 107.3 (C), 121.1 (C), 122.8 (C), 122.9 (C), 123.1 (C), 124.9 (C), 125.6 (C), 125.8 (C), 126.1 (4XC), 126.4 (C), 126.8 (C), 126.9 (C), 127.1 (C), 127.3 (C), 127.6 (2XC), 127.7 (C), 127.9 (C), 128.1 (C), 128.3 (4XC), 128.9 (C), 129.2 (C), 129.3 (2XC), 129.4 (C), 129.7 (C), 130.3 (2XC), 132.9 (C), 133.0 (C), 138.7 (C), 139.6 (C), 139.7 (C), 140.3 (2XC), 141.0 (C), 141.3 (C), 145.8 (C), 150.3 (C), 153.3 (C), 158.2 (C), 161.8 (C); HRMS (EI-ion trap) for $C_{56}H_{41}N_3O_2$ Calculated $[M^+]$ m/z: 787.3199, Observed Mass: 787.3196.

5-(4'-(1-(4-nitrophenyl)-1H-phenanthro[9,10-d]imidazol-2-yl)-[1,1'-biphenyl]-4-yl)-7,8,13,14-tetrahydrobenzo[a,i]phenanthridine (3i)

Yellow solid; (Yield 68%); Melting point: 268-270 °C; FTIR (KBr cm^{-1}): 2954, 1612, 1479, 1394, 1232, 1118, 1001, 948, 831, 750, 725, 617; 1H NMR (400 MHz, $CDCl_3$) $^{\text{TM}}$ ppm: 2.82 – 2.79 (t, 2H, J = 8 Hz, CH_2), 2.99 – 2.96 (m, 2H, CH_2), 3.19 – 3.10 (m, 4H, CH_2), 6.95 – 6.91 (t, 1H, J = 8 Hz, ArCH), 7.01 – 7.00 (d, 1H, J = 8 Hz, ArCH), 7.18 – 7.11 (m, 2H, ArCH), 7.38 – 7.28 (m, 5H, ArCH), 7.61 – 7.52 (m, 10H, ArCH), 7.71 – 7.68 (m, 3H, ArCH), 7.79 – 7.75 (m, 10H, ArCH), 7.94 – 7.93 (d, 2H, J = 4 Hz, ArCH), 8.73 – 8.71 (d, 1H, J = 8 Hz, ArCH), 8.81 – 8.79 (d, 1H, J = 8 Hz, ArCH), 8.89 – 8.87 (d, 1H, J = 8 Hz, ArCH); ^{13}C NMR $\{^1H\}$ (400 MHz, $CDCl_3$) $^{\text{TM}}$ ppm: 29.2 (CH), 29.5 (CH), 29.6 (CH), 33.2 (CH), 113.9 (C), 117.7 (C), 120.4 (C), 122.4 (C), 122.8 (C), 123.2 (C), 124.4 (C), 125.3 (C), 125.7 (C), 126.0 (C), 126.1 (2xC), 126.5 (C), 126.9 (2xC), 127.0 (2xC), 127.1 (C), 127.5 (C), 127.6 (2xC), 127.7 (C), 127.8 (C), 127.9 (C), 128.4 (2xC), 128.6 (C), 128.7 (2xC), 128.9 (2xC), 129.5 (C), 129.7 (C), 129.8 (2xC), 130.3 (C), 130.4 (C), 132.9 (C), 133.0 (C), 134.0 (C), 138.0 (C), 138.7 (C), 139.2 (C), 139.7 (C), 141.6 (C), 142.8 (C), 145.8 (C), 150.5 (C), 153.2 (C), 158.2 (C);

FULL PAPER

HRMS (EI-ion trap) for C₅₄H₃₆N₄O₂ Calculated [M⁺] m/z: 772.2838, Observed Mass: 772.2838.

5-(4'-(1-(pyridin-2-yl)-1H-phenanthro[9,10-d]imidazol-2-yl)-[1,1'-biphenyl]-4-yl)-7,8,13,14-tetrahydrodibenzo[a,i]phenanthridine (3j)

Yellow solid; (Yield 65%); Melting point: 280-282 °C; FTIR (KBr cm⁻¹): 3039, 2949, 2835, 1707, 1610, 1550, 1481, 1396, 1232, 1116, 1001, 945, 831, 748, 721, 694, 617; ¹H NMR (400 MHz, CDCl₃)TM ppm: 2.92 – 2.89 (t, 2H, J = 8 Hz), 3.08 – 3.05 (t, 2H, J = 6 Hz), 3.27 – 3.25 (t, 2H, J = 8 Hz), 3.42 – 3.39 (t, 2H, J = 8 Hz), 7.02 – 6.87 (m, 2H, ArCH), 7.17 – 7.14 (t, 3H, J = 6 Hz, ArCH), 7.51 – 7.29 (m, 19H, ArCH), 7.60 – 7.58 (d, 1H, J = 8 Hz, ArCH); ¹³C NMR {¹H} (400 MHz, CDCl₃)TM ppm: 27.1 (CH), 27.8 (CH), 27.9 (CH), 30.6 (CH), 110.3 (C), 113.1 (C), 117.9 (C), 118.7 (C), 120.9 (C), 124.8 (C), 126.2 (C), 126.8 (C), 127.4 (2XC), 127.6 (C), 127.8 (C), 128.1 (C), 128.1 (C), 128.2 (C), 128.6 (C), 128.8 (C), 128.9 (C), 129.1 (C), 129.3 (C), 129.4 (C), 129.8 (C), 130.0 (C),

130.1 (C), 130.1 (C), 130.4 (C), 130.6 (C), 120.6 (C), 130.7 (C), 130.9 (C), 131.3 (C), 131.8 (C), 131.8 (C), 132.7 (C), 133.5 (C), 137.5 (C), 138.2 (C), 138.6 (C), 141.9 (C), 143.7 (C), 143.3 (C), 144.3 (C), 144.9 (C), 153.2 (C), 156.7 (C), 160.3 (C), 160.7 (C), 161.2 (C), 161.6 (C); HRMS (EI-ion trap) for C₅₃H₃₆N₄ Calculated [M⁺] m/z: 728.2940, Observed Mass: 728.2938.

ACKNOWLEDGMENTS

The authors thanks to VIT for giving Research associate fellowship (Ref: VIT/HR/2017/5069). The authors thank to Dr. R. Srinivasan, SSL-VIT for language editing. This work was supported by the project of scientific co-operation program between Latvia, Lithuania and Taiwan "Polymeric Emitters with Controllable Thermally Activated Delayed Fluorescence for Solution-processable OLEDs" (grant No. P-LLT-19-14).

Key words: Phenanthridine. Electroluminescence. Blue luminophore. Electrochemical. Solvatochromism.

References

- [1] G. M. Farinola, R. Ragni, *Chemical Society Reviews*. **2011**, 40, 3467-3482.
- [2] a) H. Ulla, B. Garudachari, M. N. Satyanarayan, G. Umesh, A. M. Isloor, *Optical Materials*. **2014**, 36, 704-711; b) J.-H. Lee, S. H. Cheng, S. J. Yoo, H. Shin, J. H. Chang, C. I. Wu, K. T. Wong, J. J. Kim, *Advanced Functional Materials*. **2015**, 25, 342-342.
- [3] a) Q. Wang, I. W. H. Oswald, X. Yang, G. Zhou, H. Jia, Q. Qiao, Y. Chen, J. Hoshikawa-Halbert, B. E. Gnade, *Advanced Materials*. **2014**, 26, 8107-8113; b) C. Tang, R. Bi, Y. Tao, F. Wang, X. Cao, S. Wang, T. Jiang, C. Zhong, H. Zhang, W. Huang, *Chemical Communications*. **2015**, 51, 1650-1653.
- [4] a) M. A. Baldo, M. E. Thompson, S. R. Forrest, *Nature*. **2000**, 403, 750-753; b) H. Nakanotani, T. Higuchi, T. Furukawa, K. Masui, K. Morimoto, M. Numata, H. Tanaka, Y. Sagara, T. Yasuda, C. Adachi, *Nature communications*. **2014**, 5, 4016.
- [5] J. Tagare, S. Vaidyanathan, *Journal of Materials Chemistry C*. **2018**, 6, 10138-10173.
- [6] M. A. Baldo, D. F. O'Brien, Y. You, A. Shoustikov, S. Sibley, M. E. Thompson, S. R. Forrest, *Nature*. **1998**, 395, 151-154.
- [7] T. W. Lee, T. Noh, H. W. Shin, O. Kwon, J. J. Park, B. K. Choi, M. S. Kim, D. W. Shin, Y. R. Kim, *Advanced Functional Materials*. **2009**, 19, 1625-1630.
- [8] M. A. Baldo, C. Adachi, S. R. Forrest, *Physical Review B*. **2000**, 62, 10967-10977.
- [9] a) Q. Zhang, J. Li, K. Shizu, S. Huang, S. Hirata, H. Miyazaki, C. Adachi, *Journal of the American Chemical Society*. **2012**, 134, 14706-14709; b) H. Kaji, H. Suzuki, T. Fukushima, K. Shizu, K. Suzuki, S. Kubo, T. Komino, H. Oiwa, F. Suzuki, A. Wakamiya, Y. Murata, C. Adachi, *Nature communications*. **2015**, 6, 8476; c) Y. Zhao, J. Chen, D. Ma, *Applied Physics Letters*. **2011**, 99, 163303.
- [10] a) J. Yang, J. Huang, Q. Li, Z. Li, *Journal of Materials Chemistry C*. **2016**, 4, 2663-2684; b) S. Y. Lee, C. Adachi, T. Yasuda, *Advanced materials (Deerfield Beach, Fla.)*. **2016**, 28, 4626-4631; c) D. R. Lee, B. S. Kim, C. W. Lee, Y. Im, K. S. Yook, S. H. Hwang, J. Y. Lee, *ACS applied materials & interfaces*. **2015**, 7, 9625-9629; d) R. Kumar Konidena, K. R. Justin Thomas, D. Kumar Dubey, S. Sahoo, J. H. Jou, *Chemical Communications*. **2017**, 53, 11802-11805.
- [11] a) J. Tagare, H. Ulla, M. N. Satyanarayan, S. Vaidyanathan, *Journal of Photochemistry and Photobiology A: Chemistry*. **2018**, 353, 53-64; b) W. C. Chen, Y. Yuan, S. F. Ni, Q. X. Tong, F. L. Wong, C. S. Lee. **2017**, 8, 3599-3608.
- [12] a) B. Wang, X. Lv, J. Tan, Q. Zhang, Z. Huang, W. Yi, L. Wang, *Journal of Materials Chemistry C*. **2016**, 4, 8473-8482; b) C. Li, S. Wang, W. Chen, J. Wei, G. Yang, K. Ye, Y. Liu, Y. Wang, *Chemical Communications*. **2015**, 51, 10632-10635.
- [13] W. C. Chen, Y. Yuan, S. F. Ni, Z. L. Zhu, J. Zhang, Z. Q. Jiang. **2017**, 9, 7331-7338.
- [14] J. Zhao, B. Liu, Z. Wang, Q. Tong, X. Du, C. Zheng, H. Lin, S. Tao, X. Zhang, *ACS applied materials & interfaces*. **2018**, 10, 9629-9637.
- [15] A. Ivanauskaitė, R. Lygaitis, S. Raisys, K. Kazlauskas, G. Kreiza, D. Volyniuk, D. Gudeika, S. Jursenas, J. V. Grazulevicius, *Physical Chemistry Chemical Physics*. **2017**, 19, 16737-16748.
- [16] Y. Zhang, J. H. Wang, G. Han, F. Lu, Q. X. Tong, *RSC Advances*. **2016**, 6, 70800-70809.
- [17] Z. L. Zhu, M. Chen, W. C. Chen, S. F. Ni, Y. Y. Peng, C. Zhang, Q. X. Tong, F. Lu, C. S. Lee, *Organic Electronics*. **2016**, 38, 323-329.
- [18] a) Y. Kijima, N. Asai, S. I. Tamura, *Japanese Journal of Applied Physics*. **1999**, 38, 5274-5277; b) D. F. O'Brien, M. A. Baldo, M. E. Thompson, S. R. Forrest, *Applied Physics Letters*. **1999**, 74, 442-444; c) S. Naka, H. Okada, H. Onnagawa, T. Tsutsui, *Applied Physics Letters*. **2000**, 76, 197-199; d) F. Wang, J. Hu, X. Cao, T. Yang, Y. Tao, L. Mei, X. Zhang, W. Huang, *Journal of Materials Chemistry C*. **2015**, 3, 5533-5540.
- [19] M. Y. Lai, C. H. Chen, W. S. Huang, J. T. Lin, T. H. Ke, L. Y. Chen, M. H. Tsai, C. C. Wu, *Angewandte Chemie (International ed. in English)*. **2008**, 47, 581-585.
- [20] W. C. Chen, Y. Yuan, Y. Xiong, A. L. Rogach, Q. X. Tong, C. S. Lee, *ACS applied materials & interfaces*. **2017**, 9, 26268-26278.
- [21] Balijapalli, U.; Manickam, S.; Thirumoorthy, K.; Natesan Sundaramurthy, K.; Sathiyarayanan, K. I. *The Journal of Organic Chemistry*. **2019**, 84, 11513.
- [22] Z. Wang, Ping Lu, S. Chen, Zhao Gao, F. Shen, W. Zhang, Y. Xu, Hoi Sing Kwok and Y. Ma, *J. Mater. Chem.* **2011**, 21, 5451-5456.
- [23] a) S. Zhuang, R. Shangguan, J. Jin, G. Tu, L. Wang, J. Chen, D. Ma, X. Zhu, *Organic Electronics*. **2012**, 13, 3050-3059. b) C. J. Kuo, T. Y. Li, C.

FULL PAPER

- C. Lien, C. H. Liu, F. I. Wu, M. J. Huang, *Journal of Materials Chemistry*. **2009**, 19, 1865-1871.
- [24] Z. Wang, X. Li, K. Xue, H. Li, X. Zhang, Y. Liu, Z. Yu, P. Lu, P. Chen, *Journal of Materials Chemistry C*. **2016**, 4, 1886-1894.
- [25] R. J. Holmes, S. R. Forrest, Y. J. Tung, R. C. Kwong, J. J. Brown, S. Garon, M. E. Thompson, *Applied Physics Letters*. **2003**, 82, 2422-2424.
- [26] J. W. Kang, D. S. Lee, H. D. Park, Y. S. Park, J. W. Kim, W. I. Jeong, K. M. Yoo, K. Go, S. H. Kim, J. J. Kim, *Journal of Materials Chemistry*. **2007**, 17, 3714-3719.
- [27] Natesan Sundaramurthy, K.; Sathyanarayanan, K.; Aravindan, P. *Bulletin-Korean Chemical Society*. **2009**, 30, 2555.
- [28] U. Balijapalli, S. Udayadasan, E. Shanmugam, S. Kulathu Iyer, *Dyes and Pigments*. **2016**, 130, 233-244.
- [29] W. Qin, Z. Yang, Y. Jiang, J. W. Y. Lam, G. Liang, H. S. Kwok, B. Z. Tang, *Chemistry of Materials*. **2015**, 27, 3892-3901.
- [30] M. Venkatesan, K. I. Sathyanarayanan, *Sensors and Actuators B: Chemical*. **2018**, 267, 373-380.
- [31] A. Ivanauskaite, R. Lygaitis, S. Raisys, K. Kazlauskas, G. Kreiza, D. Volyniuk, D. Gudeika, S. Jursenas, J. V. Grazulevicius, *Physical Chemistry Chemical Physics*. **2017**, 19, 16737-16748.
- [32] E. Miyamoto, Y. Yamaguchi, M. Yokoyama, DENSHI SHASHIN GAKKAISHI (Electrophotography). **1989**, 28, 364-370.
- [33] Z. R. Grabowski, K. Rotkiewicz, W. Rettig, *Chemical Reviews*. **2003**, 103, 3899-4032.
- [34] M. Liu, Y. Liang, P. Chen, D. Chen, K. Liu, Y. Li, S. Liu, X. Gong, F. Huang, S. J. Su, Y. Cao, *Journal of Materials Chemistry A*. **2014**, 2, 321-325.
- [35] V. Mimaite, J. V. Grazulevicius, R. Laurinaviciute, D. Volyniuk, V. Jankauskas, G. Sini, *Journal of Materials Chemistry C*. **2015**, 3, 11660-11674.
- [36] I. Hladka, D. Volyniuk, O. Bezvikonnyi, V. Kinzhybalov, T. J. Bednarchuk, Y. Danyliv, R. Lytvyn, A. Lazauskas, J. V. Grazulevicius, *Journal of Materials Chemistry C*. **2018**, 6, 13179-13189.
- [37] a) N. C. Greenham, R. H. Friend, D. D. C. Bradley, *Advanced Materials* 1994, 6, 491-494; b) N. A. Kukhta, D. Volyniuk, L. Peciulyte, J. Ostrauskaite, G. Juska, J. V. Grazulevicius, *Dyes and Pigments*. **2015**, 117, 122-132.
- [38] N. C. Giebink, B. W. D'Andrade, M. S. Weaver, P. B. Mackenzie, J. J. Brown, M. E. Thompson, S. R. Forrest, *Journal of Applied Physics*. **2008**, 103, 044509.
- [39] J. Lee, C. Jeong, T. Batagoda, C. Coburn, M. E. Thompson, S. R. Forrest, *Nature communications*. **2017**, 8, 15566.
- [40] B. Liu, Z.-W. Yu, D. He, Z.-L. Zhu, J. Zheng, Y.-D. Yu, W.-F. Xie, Q.-X. Tong, C.-S. Lee, *J. Mater. Chem. C*. **2017**, 5, 5402-5410.
- [41] a) T. Tsutsui, *MRS Bulletin*. **2013**, 22, 39-45; b) C. A. Amorim, M. R. Cavallari, G. Santos, F. J. Fonseca, A. M. Andrade, S. Mergulhão, *Journal of Non-Crystalline Solids*. **2012**, 358, 484-491.
- [42] U. Balijapalli, S. Manickam, M. D. Thiyagarajan, S. K. Iyer, *RSC Advances* **2016**, 6, 58549-58560.
- [43] N. Zhou, S. Wang, Y. Xiao, X. Li, *Chemistry – An Asian Journal* **2018**, 13, 81-88.
- [44] Y. Tan, Z. Zhao, L. Shang, Y. Liu, C. Wei, J. Li, H. Wei, Z. Liu, Z. Bian and C. Huang, *J. Mater. Chem. C*. **2017**, 5, 11901-11909.

WILEY-VCH

Accepted Manuscript